

Observation of angular correlation between subsequently emitted Auger electrons

R. Wehlitz,* L. S. Pibida, J. C. Levin, and I. A. Sellin

Department of Physics and Astronomy, University of Tennessee, Knoxville, Tennessee 37996-1200

(Received 5 June 1998)

In an exploratory feasibility study we have measured the angular correlation between Auger electrons that were emitted in a cascadelike decay process after resonant photoexcitation, using synchrotron radiation from the Brookhaven National Synchrotron Light Source. While the monochromator was tuned to the argon $1s \rightarrow 4p$ resonance (3203.5 eV) we recorded Ar LMM Auger electrons in coincidence with $KL_{2,3}L_{2,3}$, $KL_1L_{2,3}$, and $KL_{2,3}M_{1,2,3}$ Auger electrons. We found different nonisotropic angular correlations between distinct energy regions of the LMM group of Auger lines and the $KL_{2,3}L_{2,3}$ Auger electrons, while for other kinetic energies the LMM Auger electrons exhibit isotropy. Because the KLL and LMM Auger energies are so different, we believe that the nonisotropic angular correlation observed is due to an alignment effect rather than a dynamical postcollision interaction effect. [S1050-2947(99)07801-4]

PACS number(s): 32.80.Hd

I. INTRODUCTION

Since the discovery of the Auger process [1], many experiments were performed to investigate the nonradiative deexcitation process of photoexcited atoms and ions [2]. Using synchrotron radiation, many experiments measured Auger energies, intensities, and line shapes in order to study probabilities of certain decay paths [3,4] and the so-called postcollision interaction between an Auger electron and a corresponding photoelectron [5–7]. Often, the direction of emission of an Auger electron with respect to the quantization axis, which can be either the photon-beam direction or the direction of polarization of the photon beam, was also measured to determine the influence of the “aligned” (excited) atom or ion on the direction of electron emission [8,9].

Only in a relatively few synchrotron radiation experiments was the Auger decay studied in coincidence with the emission of a photoelectron [10,11], a photon [12–14], or another Auger electron [15,11] in order to get more detailed information about particular Auger processes. The paper of Alkemper *et al.* [11] reports the decomposition of the $L_{2,3}MM$ Auger spectrum of K-ionized argon by electron-ion and electron-electron coincidence measurements, but neither detects the first-step Auger electrons nor do they measure any angle dependence of their coincidence signal. In this paper we report what we believe to be the first *angle-resolved* Auger electron–Auger electron coincidence experiment following resonant photoexcitation in which the angular correlation between subsequently emitted Auger electrons is studied [16]. For this exploratory feasibility study we have chosen a simple atom, namely, argon, that exhibits a distinguished Auger cascade, i.e., after a first Auger deexcitation the ion remains excited and undergoes another Auger decay. Such angular correlations studies proved to be a powerful tool in nuclear physics for determining angular momenta of resonances [17,18]. Here the angular correlation patterns are expected to be characteristic for particular momenta of the atomic states involved [24] and can help to identify lines.

Specifically, we photoexcited the Ar $1s$ electron to the

empty $4p$ orbital with a photon energy of 3203.5 eV [19]. In a simple picture, such an argon ion with a K -shell hole decays mainly (approximately 88%) [20] by filling the K shell with an L -shell electron giving the energy gained to another L -shell electron, which is then emitted as a so-called KLL Auger electron. Because of the two L -shell holes the Ar ion decays further, most often emitting LMM Auger electrons. Although other decay paths are possible [21,4,22], the one described above is the most probable and the one we are considering in this paper. This decay process is depicted schematically in Fig. 1. Though we note that the excited atom can also decay via emitting fluorescent light, this process contributes only approximately 11% to the total decay probability [23] and is not considered here.

The $1s \rightarrow 4p$ excitation leaves the otherwise isotropic atom in a state strongly aligned in the direction of polarization of the linearly polarized photon beam. Furthermore, in our experiment we preselect the direction of emission of the first-step (KLL) Auger electron. This introduces an additional, symmetry-breaking alignment along another axis. The total alignment is, in general, a complicated superposition of two alignments, which may result in a nonisotropic angular correlation between the KLL and LMM Auger electrons [24].

II. EXPERIMENTAL METHOD

The experiment was performed at the National Synchrotron Light Source (NSLS) at the Brookhaven National Laboratory, using photons from the bending-magnet beam line X-24A during single-bunch mode operation of the storage ring. The beam line was equipped with a germanium double-crystal monochromator providing photons from 2.5 keV to 5.4 keV, with a resolution of approximately 1 eV at a 3.2-keV photon energy. The degree of linear polarization of the photon beam was known to be higher than 95% in a horizontal direction [25], which was consistent with our measurement [(96±3)%]. Further details of the beam line are described elsewhere [26]. A sketch of our experimental setup is shown in Fig. 2.

The monochromatized and focused photon beam first passed through a 10- μ m-thick Be window that separated the

*Electronic address: wehlitz@utkux.utcc.utk.edu

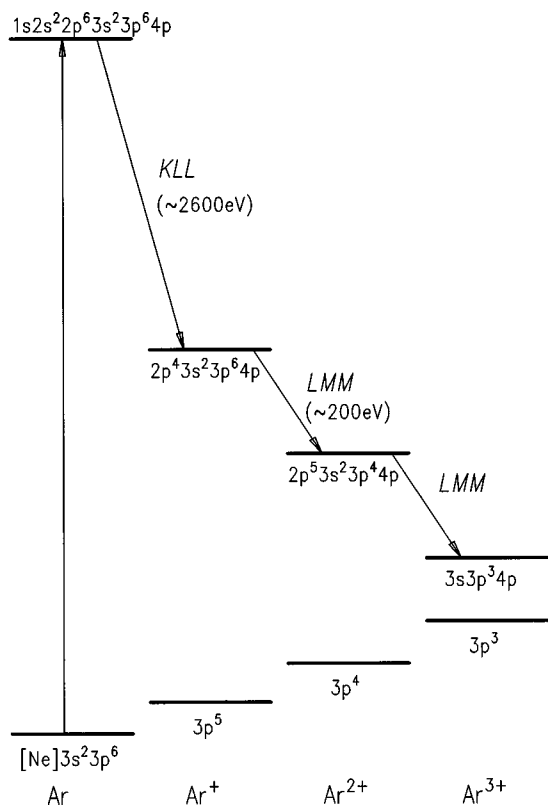


FIG. 1. Level diagram of argon showing the most probable Auger decay path after $1s \rightarrow 4p$ photoexcitation. In the first step a $KL_{2,3}L_{2,3}$ Auger electron is emitted, followed in a second and a third step by an LMM Auger electron.

vacuum of the beam line from the experimental chamber. The position of the photon beam was defined by a vertical and a horizontal slit with widths of 1 mm, respectively, upstream of the chamber. The photon beam, with its focus near the center of the experimental chamber, could be monitored and adjusted downstream with either a phosphor screen by eye or a stainless-steel plate by measuring the photoelectron current created.

The main details of the apparatus are as follows. The experimental chamber consisted of a six-way cross with a 1000-l/s turbo molecular pump and contained a hypodermic needle to inject the gas. The pressure of the residual gas was in the 10^{-6} -Pa range, rising to typically 3×10^{-3} Pa when

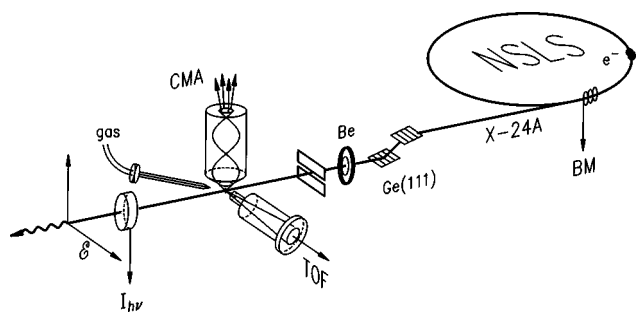


FIG. 2. Experimental setup at beam line X-24A at NSLS employing a time-of-flight (TOF) spectrometer and a cylindrical mirror analyzer (CMA) in order to take coincidence spectra. This figure shows the setup for the case in which the CMA's axis is perpendicular to the TOF spectrometer's axis.

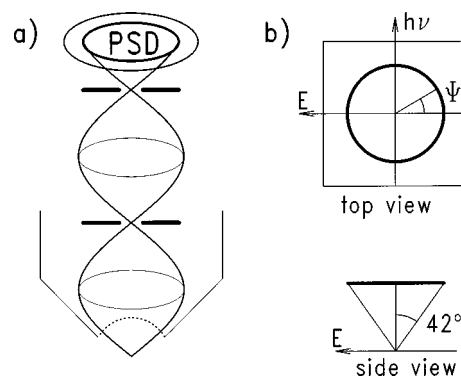


FIG. 3. How the electron's emission angle is projected onto the CMA's position-sensitive detector (PSD). (a) Sketch of our double-pass CMA with two electron trajectories passing through the CMA's apertures before hitting the PSD. (b) Sketch of the PSD's image. The detection position is given by the angle ψ (see the text for details).

the sample gas was admitted. The effusive gas jet intersected the photon beam at the center of the chamber defining the interaction region. The inside of the chamber was lined with μ metal to reduce magnetic fields in the chamber, thereby also reducing the effect on electron trajectories to an acceptably low value.

Two electron spectrometers were mounted on the chamber to determine the kinetic energy and direction of the electrons created in the interaction region. One spectrometer was an angle-resolving double-pass cylindrical mirror analyzer (CMA). The CMA, equipped with a position-sensitive detector (PSD) mounted downstream of its energy selection aperture, permitted registering not only the energy, but also the azimuthal and polar angles of KLL and KLM Auger emission in the interaction region, which is imaged 1 to 1 in the CMA image space, for all azimuthal angles (with respect to the CMA axis) and a band of polar angles simultaneously. The CMA's axis was always aligned perpendicular to the photon beam, in one experiment parallel and in a second experiment perpendicular to the electric vector of the photon beam. The CMA accepted electrons emerging from the interaction region in a cone with a $\pm 42.3^\circ$ opening angle with a width of $\pm 3^\circ$. Although the angular resolution, which is given by the spatial resolution of our PSD, is better than $\pm 3^\circ$, we integrated the intensity over this width in the experiment presented here. The orientation of the CMA's axis could be adjusted under vacuum to optimize the intensity and spatial distribution of the PSD signal. All events form a circular image on the PSD, as is seen in Fig. 3. From the position of such an event within the PSD's circular image we could calculate unambiguously the direction of the electron when it has left the interaction region by simple formulas [27]. The events were preamplified and analyzed by a commercial image particle detector module.

The second spectrometer was an electron time-of-flight (TOF) spectrometer, which was always mounted perpendicular to the photon beam and parallel to the direction of the electric vector of the photon beam. In one experiment the CMA was located coaxially with the TOF spectrometer, while in a second experiment its axis was oriented perpendicular to the axis of the TOF (see Fig. 2). The TOF spectrometer has a flight path of 460 mm, an energy resolution of

about 2% of the kinetic energy of the electron, and an acceptance angle of $\pm 2.6^\circ$. While the interaction region was free of electric fields, the electrons were accelerated by 5 V or retarded by 90 V after entering the TOF's entrance aperture, located 28 mm away from the interaction region. The position of the entrance aperture could be adjusted under vacuum to optimize the intensity of the TOF spectrum. The flight path was pumped by a 70-l/s turbo molecular pump to avoid inelastic scattering of electrons at the gas in the TOF spectrometer. The flight path was shielded with μ metal from magnetic fields to reduce transmission losses within the spectrometer. The electrons were detected by two 40-mm microchannel plates in a chevron-like mounting and their flight time was measured with respect to a fast timing signal (bunch marker) provided by the storage ring. Details of the electron TOF spectrometer can be found elsewhere [28].

Energy-selected Auger electrons were collected with the CMA at a variety of angles relative to the axis of the TOF spectrometer, which was employed to take a coincidence spectrum of a group of Auger lines simultaneously. In the noncoincident mode the timing signal of the storage ring was used to take TOF spectra, while in the coincident mode the signal of the CMA's PSD was used in addition to the timing signal such that electrons were detected by the TOF spectrometer only if another electron was detected before by the PSD.

Our data acquisition program stored all relevant information in "list" mode [29]. This means that information pertaining to each event, such as flight time and the X and Y positions on the PSD, is recorded and stored sequentially, so that data belonging to particular experimental parameters can later be extracted according to software preferences. We note that our coincidence setup enables us to record the noncoincident as well as coincident TOF spectra simultaneously; details of this coincidence setup are described in Ref. [27].

III. RESULTS AND DISCUSSION

Figure 4 shows noncoincident Auger spectra of argon after resonant $1s \rightarrow 4p$ photoexcitation at $h\nu = 3203.5$ eV. The most prominent Auger transition is $KL_{2,3}L_{2,3}$, which was chosen for measuring the angular correlation between Auger electrons for the sake of sufficient intensity of the coincidence signal. The LMM group of Auger lines is shown in Fig. 4(b) and was taken using the CMA in retardation mode with a pass energy of 25 eV, showing the complex line structure of the LMM Auger group in detail. No detailed assignments of the individual resonant Auger lines are available. In order to make a tentatively rough assignment of the resonant $L_{2,3}MM$ Auger region we performed a least-squares fit using the nonresonant, electron-impact excited spectrum of Werme *et al.* [30]. The resulting simulated spectrum is shown as a dotted line in Fig. 4(b). As was shown in Refs. [4,11], the $L_{2,3}MM$ Auger spectrum after $1s$ ionization consists in a first approximation of partial spectra that are similar to an electron-impact excited spectrum dominated by the $L_{2,3}MM$ diagram lines. We have used in total six electron-impact excited Auger spectra as a fit model for our resonant Auger spectrum, which consists mainly of three groups, in contrast to the corresponding nonresonant Auger spectrum after $1s$ ionization, which consists mainly of five groups [11]. Each

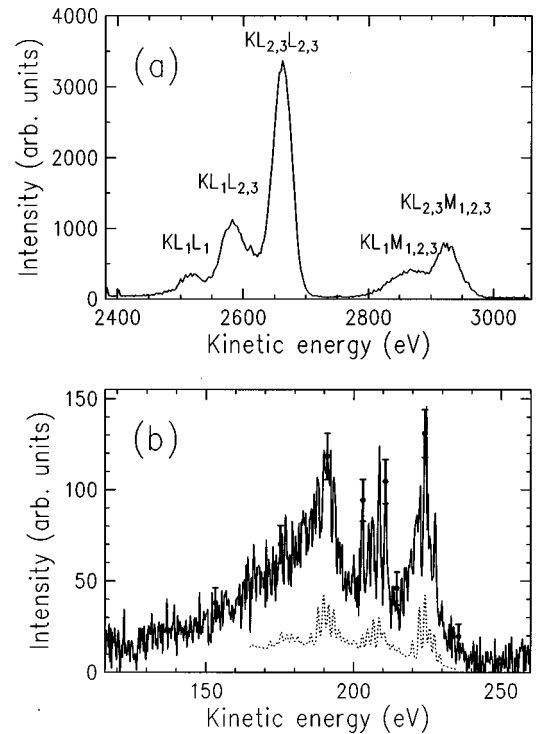


FIG. 4. Auger spectra of argon after resonant $1s \rightarrow 4p$ photoexcitation at $h\nu = 3203.5$ eV. (a) KLL and KLM Auger lines taken with our CMA. (b) Group of LMM Auger lines subsequently emitted after the KLL Auger electrons taken with the CMA using a pass energy of 25 eV (solid line). Some error bars are shown to visualize the uncertainty of the intensity. The dotted line is a simulated spectrum in order to identify the groups of Auger lines as described in the text. This spectrum is displayed on a different intensity scale to avoid overlap with the measured spectrum.

of the three groups was modeled by two electron-impact excited spectra [30] with a separation of approximately 3.5 eV respectively. This energy splitting may be due to the $4p$ spectator electron. Comparing our results with the findings of Alkemper *et al.* [11], we tentatively assign the high-energy part of the $L_{2,3}MM$ Auger lines (215–233 eV) to $L_{2,3}M_{2,3}M_{2,3}$ transitions with a spectator hole in the L shell. The low-energy part (183–196 eV) consists mainly of the "third-step" Auger decay or, in other words, the second $L_{2,3}M_{2,3}M_{2,3}$ transition after the first L -shell hole was filled in a previous LMM Auger transition. This decay takes place in the presence of two holes in the M shell. The medium-energy part may consist of several Auger transitions that are not part of the decay cascade that starts with a $KL_{2,3}L_{2,3}$ transition (including diagram lines). However, it also includes $LM_{1M_{2,3}}$ transitions taking place after a $KL_{2,3}L_{2,3}$ transition in the first step.

The coincident spectra were taken with the TOF spectrometer, which had to be used in low-resolution mode, sacrificing the energy resolution in order to achieve an adequate coincident count rate, compatible with the flux available on NSLS beam line X-24A. Despite this essential resolution compromise, the overall coincident count rate was still only about 40 mHz in the case of selecting $KL_{2,3}L_{2,3}$ Auger electrons and we had to collect and add up several coincidence spectra to get an intensity sufficient for data analysis. We also recorded LMM coincidence spectra following the

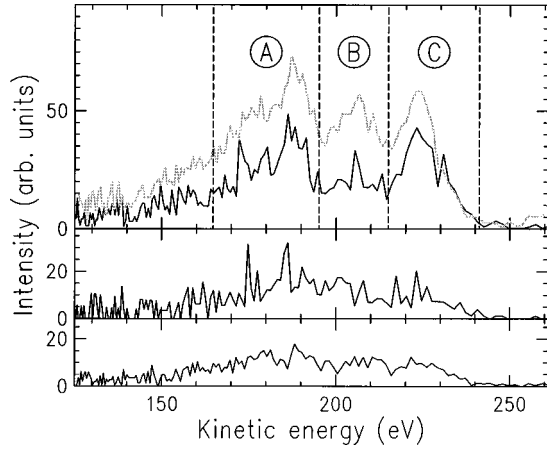


FIG. 5. Three coincidence spectra of the Ar LMM Auger region taken with our TOF spectrometer while the CMA's axis was perpendicular to the axis of the TOF spectrometer, i.e., the relative angle between the electron emission directions varies between 132° and 48° . Lower panel, in coincidence with $KL_1L_{2,3}$ Auger electrons; middle panel, in coincidence with $KL_{2,3}M_{1,2,3}$ Auger electrons; upper panel, in coincidence with $KL_{2,3}L_{2,3}$ Auger electrons. The gray line shows the noncoincident spectrum arbitrarily scaled for comparison. For further analysis this Auger spectrum was cut into three energy slices (A, B, and C) as indicated by the vertical lines.

$KL_1L_{2,3}$ and $KL_{2,3}M_{1,2,3}$ Auger decays as shown in Fig. 5. In these cases the count rate was too low to determine an angular correlation but, nevertheless, differences in the structure of the group of LMM Auger lines due to the selection of a specific first-step Auger decay can be seen, particularly between the $KL_{2,3}L_{2,3}$ and the two other coincidence spectra.

As mentioned in the Introduction, the resonant $1s \rightarrow 4p$ excitation aligns the argon atom along the polarization vector of the photon beam. However, if the $4p$ electron does not participate in the decay process and interacts only weakly with the core electrons, i.e., the so-called strict spectator model is valid [34], then the emission of a KLL Auger electron is expected to be isotropic since the $1s$ hole is isotropic in spite of the strong alignment. Employing the CMA we have determined the (noncoincident) angular distribution of the three groups of KLL and the two groups of KLM Auger electrons on resonance. Indeed we have measured an isotropic angular distribution with β values between -0.10 and 0.07 with an error of 0.15 , proving that the $4p$ electron does not significantly influence the first-step Auger decay. Also the angular distribution of the total LMM Auger group was measured to be almost isotropic with $\beta=0.25(30)$. Because of the rather big error bar, it is not clear whether the strict spectator model holds, as in the case of Ar $2p \rightarrow 4s$ excitations [31], or fails, as in the case for magnesium [32]. The angular distribution of the three major parts of the LMM Auger group was determined to be the same within an error of 0.1β units. The general term ‘‘spectator model’’ means that the decaying inner-shell hole is not filled by the excited electron but remains in its excited state [8]. An even simpler model, the so-called *strict* spectator model [33], assumes that the interaction between the spectator electron (here $4p$) and the core electrons is so weak that it can be ignored [34]. The strict spectator model permits relating the angular distribu-

tion of the normal Auger lines to that of the resonant Auger lines. In our case the interaction of the $4p$ spectator electron cannot be neglected regarding the intensity distribution of the LMM Auger lines as can be seen by comparing our resonant Auger spectrum with the corresponding nonresonant Auger spectra of Refs. [35,11]. The overall Auger line structure is different; while the nonresonant $L_{2,3}MM$ Auger spectrum consist of mainly five groups of lines, the resonant spectrum has only three groups of lines at slightly different kinetic energies. However, this situation is similar to the Ar $2p \rightarrow 4s$ case [31], where the positions and intensities of Auger lines are different for the resonant and nonresonant excitation. Nevertheless, the strict spectator model is still valid regarding the angular distribution of the resonant Auger lines [31] as it appears to be in our case.

Detecting the $KL_{2,3}L_{2,3}$ Auger electron in *coincidence* with an LMM Auger electron introduces another anisotropy along the direction of emission of the first-step Auger electron to our system. This anisotropy is not connected with any dynamical effect, such as postcollision interaction, but is instead a consequence of angular momentum conservation. Since the coincidence data were acquired in list mode, as mentioned above, we determined for each LMM Auger electron the direction of the corresponding $KL_{2,3}L_{2,3}$ Auger electron.

Because of the particular geometry of our experiment (the LMM Auger electron was always detected along the axis of polarization), we have axial symmetry along this axis and hence no possibility of observing forward-backward asymmetry with respect to the photon beam direction. Therefore, the angular distribution of the intensity I of the KLL Auger electrons measured in coincidence with the subsequently emitted LMM Auger electrons will be axially symmetric and can be described in general by two parameters β_2 and β_4 [24]:

$$I \sim 1 + \beta_2 P_2[\cos(\rho)] + \beta_4 P_4[\cos(\rho)], \quad (1)$$

with ρ , the angle between the two Auger electrons and P_2 and P_4 , the second- and fourth-order Legendre polynomials, respectively. The angle ρ can be calculated from the angle ψ of the PSD image using the formula

$$\rho = 90^\circ + \arctan[\cos(\psi)\tan(\omega)], \quad (2)$$

with ω half the opening angle of the CMA's acceptance cone (42.3°). In the case where the CMA was mounted opposite the TOF spectrometer, we have only one *fixed* angle ρ between the detected Auger electrons, which was $180^\circ - 42.3^\circ = 137.7^\circ$. When the axis of the CMA was perpendicular to the TOF spectrometer, we collected electrons of all angles ρ between $90^\circ - 42.3^\circ = 47.7^\circ$ and $90^\circ + 42.3^\circ = 132.3^\circ$. In fact, we integrated over $10^\circ - 20^\circ$ regions of the PSD image adding the intensity in the forward and corresponding backward directions with respect to the photon beam direction, making use of the axial symmetry as mentioned above. Each angle slice was corrected with the spatial detection efficiency of the PSD determined with the noncoincident Ar KLL signal above the $1s$ threshold since this signal is isotropic. This procedure also permits a correction for the different sizes of angle slices. The false coincidences were subtracted from the coincidence spectra for each angle

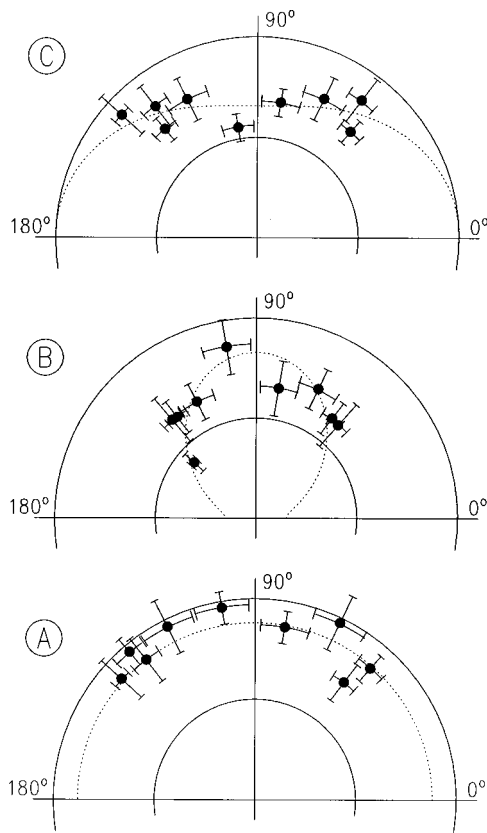


FIG. 6. Polar plots showing the angular correlation between the Ar $KL_{2,3}L_{2,3}$ Auger electrons and three different energy regions (as shown in the upper panel of Fig. 5) of subsequently emitted LMM Auger electrons. The radius represents the intensity of the particular LMM Auger region while the angle ρ , as defined in Eq. (2), represents the relative emission angle of the $KL_{2,3}L_{2,3}$ Auger electron with respect to the LMM Auger electrons detected at 0° . The LMM Auger electrons were always detected in the direction of the electric vector of the photon beam at 0° . Upper panel, region C; middle panel, region B; lower panel, region A. The dotted lines are curves fitted to the data points.

slice, normalized with the intensity of the KLL Auger electron intensity for the same angle slice.

Although it is desirable to investigate individual Auger lines, we had to integrate the intensity of kinetic-energy regions because of the low coincidence signal. Therefore, the group of LMM Auger lines was divided into three energy regions, as discussed above, each of which has sufficient intensity to produce a coincidence spectrum at adequate statistics. These energy regions are marked by dashed lines in Fig. 5. The result of this data analysis is shown in Fig. 6. While the energy region A (as marked in Fig. 5), which consists mainly of the second $L_{2,3}MM$ Auger decay in the pres-

ence of a double M -shell hole, shows no or only little anisotropic angular correlation, region B, which represents mainly $L_{2,3}M_1M_{2,3}$ Auger transitions, shows a pronounced anisotropy. Region C, consisting of $L_{2,3}M_{2,3}M_{2,3}$ Auger transitions in the presence of an L -shell hole, exhibits a small anisotropy. The intensity of region B is highest when the $KL_{2,3}L_{2,3}$ Auger electron is ejected at 90° with respect to the LMM Auger electron. We applied Eq. (1) to the data and found $\beta_2 = -0.7(2)$ with β_4 close to zero. However, it is also possible that there is some unobserved intensity along the direction of the electric vector. In contrast, the intensity of region C is smallest when the $KL_{2,3}L_{2,3}$ Auger electron is ejected at 90° . In this case we obtain a $\beta_2 = +0.3(2)$ when β_4 is set to zero. However, in order to compare calculations with the experimental results, a higher-energy resolution for the LMM Auger group is desirable.

IV. CONCLUSIONS

In summary, we have demonstrated in this study the cascade Auger angular correlation technique. We have measured the angular correlation between subsequently emitted Auger electrons after resonant $1s \rightarrow 4p$ photoexcitation of argon. Time-of-flight spectra of the LMM group of Auger lines were taken in coincidence with the corresponding $KL_{2,3}L_{2,3}$, $KL_1L_{2,3}$, and $KL_{2,3}M_{1,2,3}$ Auger electron emitted at different angles with respect to the LMM Auger electron. The LMM Auger spectrum taken in coincidence with the corresponding $KL_{2,3}L_{2,3}$ Auger electron showed, depending on the energy region, an isotropic as well as a nonisotropic angular correlation. We observed for the high-energy part (215–242 eV) of the LMM Auger group a small and for the medium energy part (196–215 eV) a pronounced anisotropic angular correlation, while the lower-energy region (165–196 eV) shows an isotropic angular correlation to the KLL Auger electron. Interestingly, the anisotropic angular correlations of the medium- and high-energy parts are very different. Because of the low-energy resolution, individual Auger lines could not be examined, but in future experiments with a higher photon flux and better electron energy resolution one might be able to compare experimental results with theoretical calculations for specific decay paths.

ACKNOWLEDGMENTS

The authors wish to thank the staff of the NSLS, particularly B. A. Karlin, for their excellent support. We are also thankful to Professor N. M. Kabachnik for many fruitful discussions. This work was supported by the National Science Foundation and the U.S. Department of Energy. R.W. gratefully acknowledges the A. v. Humboldt Foundation for financial support.

[1] P. Auger, *J. Phys. Radium* **6**, 205 (1925).

[2] H. Aksela, S. Aksela, and N. M. Kabachnik, in *VUV and Soft X-Ray Photoionization*, edited by U. Becker and D. A. Shirley (Plenum, New York, 1996), p. 401, and references therein; W. Mehlhorn, in *Atomic Inner Shell Physics*, edited by B. Crase-

mann (Plenum, New York, 1985), p. 119.

[3] M. O. Krause, *J. Phys. (Paris)*, Colloq. **32**, C4-76 (1971).

[4] F. v. Busch, J. Doppelfeld, C. Günther, and E. Hartmann, *J. Phys. B* **27**, 2151 (1994).

[5] V. Schmidt, in *X-Ray and Atomic Inner-Shell Physics*, edited

- by B. Crasemann, AIP Conf. Proc. No. 94 (AIP, New York, 1982), p. 544.
- [6] S. Southworth, U. Becker, C. M. Truesdale, P. H. Kobrin, D. W. Lindle, S. Owaki, and D. A. Shirley, Phys. Rev. A **28**, 261 (1983).
- [7] H. Kjeldsen, T. D. Thomas, P. Lablanquie, M. Lavollée, F. Penent, M. Hochlaf, and R. I. Hall, J. Phys. B **29**, 1689 (1996).
- [8] U. Hergenhahn and U. Becker, J. Electron Spectrosc. Relat. Phenom. **72**, 243 (1995).
- [9] H. Aksela, J. Jauhianen, E. Kukk, E. Nõmmiste, S. Aksela, and J. Tulkki, Phys. Rev. A **53**, 290 (1996).
- [10] B. Kämmerling and V. Schmidt, Phys. Rev. Lett. **67**, 1848 (1991).
- [11] U. Alkemper, J. Doppelfeld, and F. von Busch, Phys. Rev. A **56**, 2741 (1997).
- [12] S. H. Southworth, M. A. MacDonald, T. LeBrun, and R. D. Deslattes, Nucl. Instrum. Methods Phys. Res. A **347**, 499 (1994).
- [13] U. Arp, J. W. Cooper, T. LeBrun, S. H. Southworth, M. Jung, and M. A. MacDonald, J. Phys. B **29**, L837 (1996).
- [14] H.-J. Beyer, J. B. West, K. J. Ross, K. Ueda, N. M. Kabachnik, H. Hamdy, and H. Kleipoppen, J. Phys. B **28**, L47 (1995).
- [15] E. v. Raven, M. Meyer, M. Pahler, and B. Sonntag, J. Electron Spectrosc. Relat. Phenom. **52**, 677 (1990).
- [16] N. M. Kabachnik, in *Proceedings of the International Workshop on Photoionization 1992*, edited by U. Becker and U. Heinzmann (AMS, New York, 1993), pp. 20–23.
- [17] S. Devons and L. J. B. Goldfarb, in *Nuclear Reactions III*, edited by S. Flügge, Handbuch der Physik, Vol. 42 (Springer-Verlag, Berlin, 1957), p. 362.
- [18] A. J. Ferguson, *Angular Correlation Methods in Gamma-Ray Spectroscopy* (North-Holland, Amsterdam, 1965).
- [19] M. Breinig, M. H. Chen, G. E. Ice, F. Parente, B. Crasemann, and G. S. Brown, Phys. Rev. A **22**, 520 (1980).
- [20] L. Asplund, P. Kelfve, B. Blomster, H. Siegbahn, and K. Siegbahn, Phys. Scr. **16**, 268 (1977).
- [21] K. Ueda, E. Shigemasa, Y. Sato, A. Yagishita, M. Ukai, H. Maezawa, T. Hayaishi, and T. Sasaki, J. Phys. B **24**, 605 (1991).
- [22] T. Hayaishi, E. Murakami, E. Shigemasa, A. Yagishita, F. Koike, and Y. Morioka, J. Phys. B **28**, 5261 (1995).
- [23] M. O. Krause, J. Phys. Chem. Ref. Data **8**, 307 (1979).
- [24] N. M. Kabachnik, in *X-Ray and Inner-Shell Processes*, edited by R. L. Johnson, B. F. Sonntag, and H. Schmidt-Böcking, AIP Conf. Proc. No. 389 (AIP, Woodbury, NY, 1997), p. 689.
- [25] B. Krässig, M. Jung, D. S. Gemmell, E. P. Kanter, T. LeBrun, S. H. Southworth, and L. Young, Phys. Rev. Lett. **75**, 4736 (1995).
- [26] P. L. Cowan, S. Brennan, R. D. Deslattes, A. Henins, T. Jach, and E. G. Kessler, Nucl. Instrum. Methods Phys. Res. A **246**, 154 (1986); B. A. Karlin, P. L. Cowan, and J. C. Woicik, Rev. Sci. Instrum. **63**, 526 (1992).
- [27] R. Wehlitz, L. S. Pibida, J. C. Levin, and I. A. Sellin (unpublished); L. S. Pibida, Ph.D. thesis, University of Tennessee, 1997 (unpublished).
- [28] O. Hemmers, S. B. Whitfield, P. Glans, H. Wang, D. W. Lindle, R. Wehlitz, and I. A. Sellin (unpublished).
- [29] The data acquisition program and corresponding CAMAC modules were developed by Dr. Leif Liljeby of the Manne Siegbahn Laboratory (Sweden).
- [30] O. Werme, T. Bergmark, and K. Siegbahn, Phys. Scr. **8**, 149 (1973).
- [31] B. Langer, N. Berrah, A. Farhat, M. Humphrey, D. Cubaynes, A. Menzel, and U. Becker, J. Phys. B **30**, 4255 (1997).
- [32] U. Hergenhahn, S. B. Whitfield, J. Tulkki, F. Heiser, N. M. Kabachnik, B. Langer, and U. Becker, Phys. Rev. A **55**, 2050 (1997).
- [33] U. Hergenhahn, B. Lohmann, N. M. Kabachnik, and U. Becker, J. Phys. B **26**, L117 (1993).
- [34] H. Aksela, S. Aksela, and N. M. Kabachnik, in *VUV and Soft X-Ray Photoionization* (Ref. [2]), p. 428.
- [35] S. H. Southworth, M. A. MacDonald, T. LeBrun, Y. Azuma, and J. W. Cooper, in *Atomic Physics at High Brilliance Synchrotron Sources*, Proceedings of a Workshop held at Argonne National Laboratory, 1994, edited by G. Berry, P. Cowan, and D. Gemmel (Argonne National Laboratory, Argonne, 1994), p. 211.